

Manufacturing Technology

**Kenneth L. Blaedel,
Thrust Area Leader**

This is an informal report intended primarily for internal or limited external distribution. The opinions and conclusions stated are those of the author and may or may not be those of the Laboratory.

Work performed under the auspices of the U.S. Department of Energy by Lawrence Livermore National Laboratory under Contract W-7405-Eng-48.

January 1998

Disclaimer

This document was prepared as an account of work sponsored by an agency of the United States Government. Neither the United States Government nor the University of California nor any of their employees, makes any warranty, express or implied, or assumes any legal liability or responsibility for the accuracy, completeness, or usefulness of any information, apparatus, product, or process disclosed, or represents that its use would not infringe privately owned rights. Reference herein to any specific commercial products, process, or service by trade name, trademark, manufacturer, or otherwise does not necessarily constitute or imply its endorsement, recommendation, or favoring by the United States Government or the University of California. The views and opinions of authors expressed herein do not necessarily state or reflect those of the United States Government or the University of California, and shall not be used for advertising or product endorsement purposes.

This report has been reproduced
directly from the best available copy.

Available to DOE and DOE contractors from the
Office of Scientific and Technical Information
P.O. Box 62, Oak Ridge, TN 37831
Prices available from (615) 576-8401, FTS 626-8401

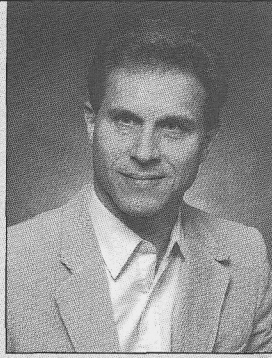
Available to the public from the
National Technical Information Service
U.S. Department of Commerce
5285 Port Royal Rd.,
Springfield, VA 22161

Manufacturing Technology

**Kenneth L. Blaedel,
Thrust Area Leader**

Reprinted from Engineering Research, Development and Technology
FY 97 UCRL 53868-97

January 1998



Kenneth L. Blaedel, Thrust Area Leader

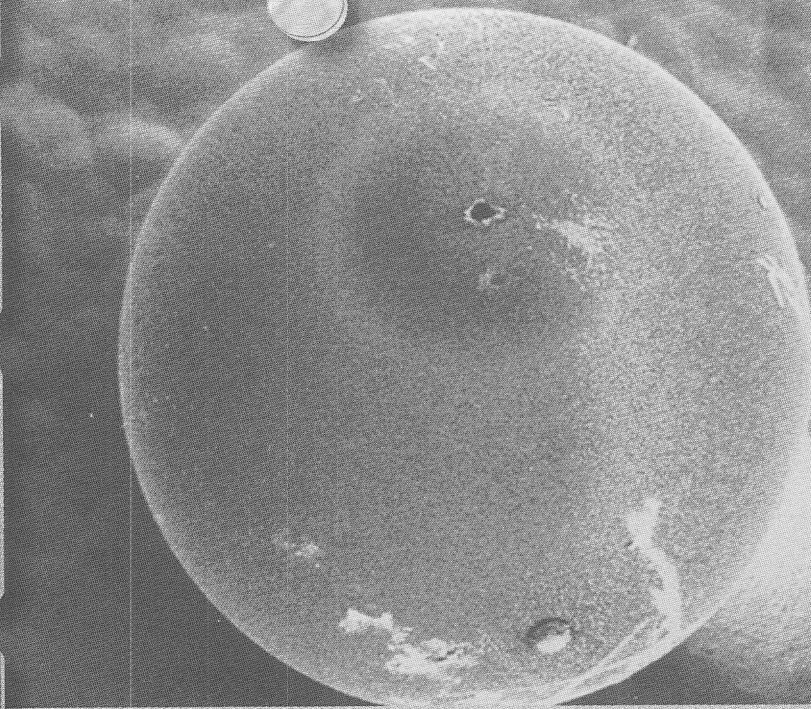
The mission of the Manufacturing Technology thrust area at Lawrence Livermore National Laboratory (LLNL) has been to have an adequate base of manufacturing technology, not necessarily resident at LLNL, to conduct our future business.

Our specific goals were (1) to develop an understanding of fundamental fabrication processes; (2) to construct general purpose process models that have wide applicability; (3) to document our findings and models in journals; (4) to transfer technology to LLNL programs, industry, and colleagues; and (5) to develop continuing relationships with the industrial and academic communities to advance our collective understanding of fabrication processes.

In support of this mission, two projects are reported here, each of which explores a way to bring higher precision to the manufacturing challenges that we face over the next few years. The first, "A Spatial-Frequency-Domain Approach to Designing a Precision Machine Tools," is an overall view of how we design machine tools and instruments to make or measure workpieces that are specified in terms of the spatial frequency content of the residual errors of the workpiece surface. This represents an

improvement of an "error budget," a design tool that saw significant development in the early 1980's, and has been in active use since then. The second project, "Micro-Drilling of ICF Capsules," is an attempt to define the current state in commercial industry for drilling small holes, particularly laser-drilling. The report concludes that 1- μ m-diameter holes cannot currently be drilled to high aspect ratios, and then defines the engineering challenges that will have to be overcome to machine holes small enough for NIF capsules.

Looking to the future, the Engineering Directorate is implementing a new technology plan, which calls for transitioning the thrust areas into centers. One such center will be in precision engineering and will serve to further focus our manufacturing efforts on precision, as well as to merge the different projects into a more comprehensive and cohesive effort. The Precision Engineering Center will play a more active role in directly enabling the success of LLNL programs, and will bring focus to Engineering's investment in technology development.



Manufacturing Technology

4

4. Manufacturing Technology

Overview

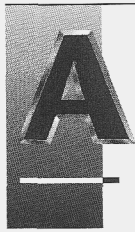
Kenneth L. Blaedel, Thrust Area Leader

A Spatial-Frequency-Domain Approach to Designing Precision Machine Tools

Debra A. Krulewich4-1

Micro-Drilling of ICF Capsules

Steven A. Jensen4-13



Spatial-Frequency-Domain Approach to Designing Precision Machine Tools

Debra A. Krulewich

*Manufacturing and Materials Engineering Division
Mechanical Engineering*

The goal of this project is to develop a new error budgeting methodology for designing machine tools and motion control systems that can meet increasingly stringent tolerances. This new approach quantitatively accounts for the spatial and temporal frequency content of the error sources during a machining process and estimates workpiece error in terms of power spectral density (PSD). In our methodology, the amplitude and frequency content of the contributing error terms are appropriately summed. Compared to the traditional approach, this method is better able to handle the dynamics of the machining, producing a mapping of the PSD onto the machined workpiece. During FY97, three key technical issues have been analyzed: 1) identifying and characterizing elemental error terms that contribute to the net error; 2) developing a combinatorial rule to sum the elemental error terms; and 3) developing a frequency domain transfer function of the machining process to map the PSD onto the machined workpiece.

Introduction

Increased precision in manufacturing is being demanded by Lawrence Livermore National Laboratory (LLNL) programs, in areas ranging from National Ignition Facility (NIF) optics¹ manufacturing and Inertial Confinement Fusion (ICF) target positioning, to the production and alignment of optics for extreme ultra-violet (EUV) lithography.² Other LLNL areas that drive unique requirements for precision include the machining of diffractive optical systems, the fabrication of ICF targets,³ and the manufacture of weapons components.

The precision-to-cost ratio is another metric that relates to a wide variety of industrial mechanical systems, such as automotive engine components, but has a special significance at LLNL where an increased interest in tighter tolerances is matched by the need to lower program costs. Minimizing technical risk is another issue that defines manufacturing goals for programs that cannot tolerate yield factors less than 100%, such as in fabricating components for the nuclear weapons program.

This project will significantly improve the process of formulating an error budget for a manufacturing, positioning, or measurement system. Error budgets provide the formalism to account for all sources of uncertainty in a process, and sum them to arrive at a net prediction of how 'precisely' a manufactured

component can meet a target specification. The error budgeting process drives decisions regarding the conceptual design of the system and choice of components and sub-systems, and enables a rationale for balancing precision (performance), cost, and risk.

The basic procedure of preparing an error budget begins by considering the amplitudes of all terms that contribute to the error motion of a machine.⁴⁻¹⁰ These are summed using a combinatorial algorithm¹¹⁻¹³ that produces an estimate of the net displacement error in a given direction. This net error can be compared to a mechanical specification, or further related to a workpiece by considering the machining operation and its associated transfer function. Once the error budget is transformed to relevant workpiece coordinates, it can be compared to a specified workpiece tolerance.

This methodology is quite successful when the desired errors in tool positioning are characterized by a single number, designated by either an rms or peak-to-valley value. However, recent specifications for advanced optical systems are being posed in terms of the spatial frequency content of the residual errors imparted to the optical wavefront. This requirement directly maps back to specifications for workpiece accuracy posed in terms of the power spectral density (PSD)¹⁴ of the workpiece surface errors. Similarly, the ability of the physics

community to better model implosion events is leading to manufacturing specifications for structural weapons components in terms of the spatial frequency of the residual errors on the surface.

Based on these requirements, it is no longer acceptable to specify manufacturing or machine tool tolerances in terms of a single number that spans all temporal and spatial frequencies. Current efforts to embrace the frequency aspects of error budgeting typically divide the frequency spectrum into a small number of bins, such as figure, ripple, and finish, and then perform an error budget summation within each of those bins. This may be acceptable when the manufacturing specifications can be simplified to 2 to 3 frequency bins. However, this approach does not satisfy the demand for a continuous PSD of the dimensional errors on the machined part.

The goal of this project is to develop a new error budgeting methodology for designing machine tools and motion control systems that can meet increasingly stringent tolerances. This new approach quantitatively accounts for the spatial and temporal frequency content of the error sources during a machining process and estimates workpiece error in terms of PSD.

Figure 1 shows the proposed error budget flowchart that uses frequency information for the error sources. Similar to the traditional approach, the error sources, S , couple to the machine via mechanisms, C , resulting in displacements, Δ . These displacements are not converted to a single number,

but are transformed into PSDs for each of the elemental errors; for example, PSD_{1x} . The elemental PSDs are then summed using an appropriate combinatorial algorithm, which has been defined during FY-97 and will be described in detail in the next section.

The results of this summation are the net PSDs for each relevant machine coordinate and their probability density functions. With this information, confidence intervals around the expected errors can be determined. The final box on the flowchart of Fig. 1 is a transfer function, T_{ij} , which accounts for the frequency response of the machining operation, and yields the error spectrum that would be produced on the workpiece.

Progress

We have proposed to test the hypothesis that the composite PSD of the dimensional errors on a workpiece can be predicted by appropriately combining the PSDs of the machine's elemental errors. The practical consequence of this hypothesis is that a machine tool could be designed for meeting a programmatic PSD specification. We have made significant progress toward this goal during the first part of FY-97.

The project tasks are broadly divided between analysis and validation experiments. During FY-97, we have concentrated our efforts on analysis. Key technical issues include: 1) identifying and

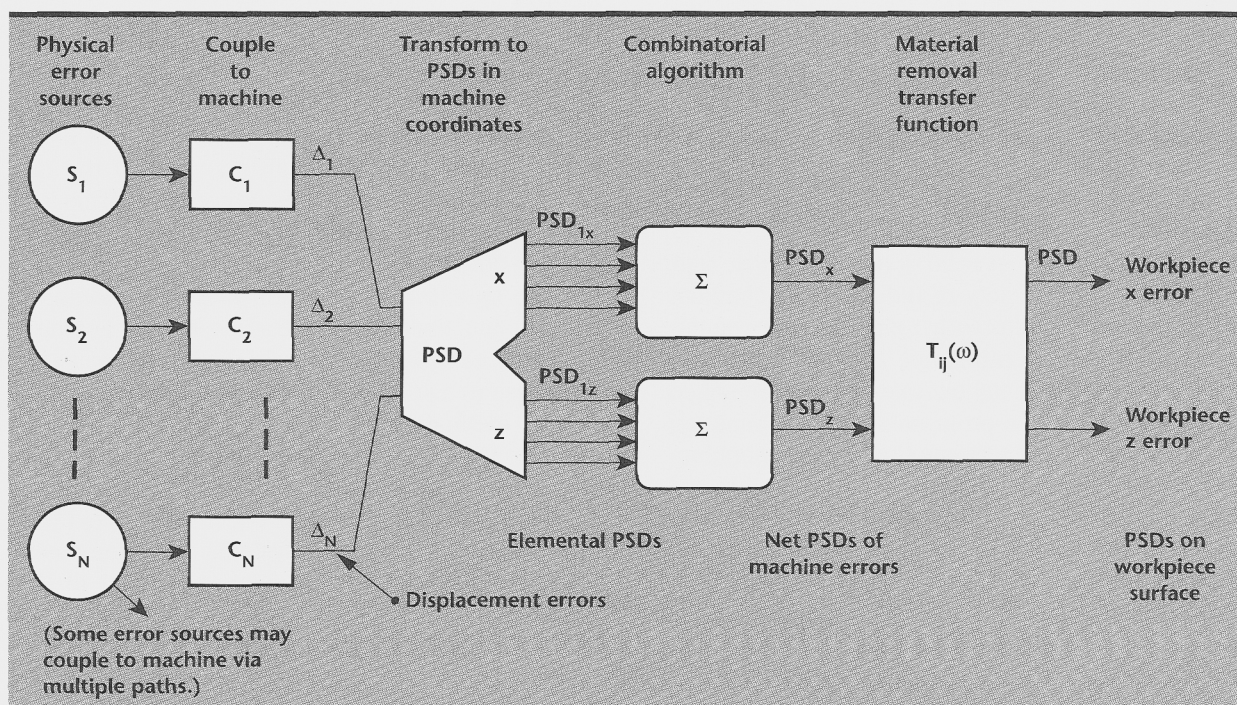


Figure 1. Proposed error budget flowchart using frequency information for the error sources.

characterizing elemental error terms that contribute to the net error; 2) developing a combinatorial rule to sum the elemental error terms; and 3) developing a frequency domain transfer function of the machining process to account for the dynamics during cutting. Progress on these issues will be discussed in detail.

We began the project by reviewing PSD requirements for a variety of programs, including the manufacture of ICF targets and KDP crystals for NIF, and structural weapons components for the Life Extension Programs. We also performed a literature search to identify current work in this area. We located many papers discussing traditional error budget methodology and combinatorial rules, but no papers were found that specifically addressed frequency domain error budgeting techniques. We did not locate anyone who has studied the distribution of particular elemental error terms, nor their frequency content. Furthermore, we did not locate any sources that discussed how to sum elemental error PSDs to predict a net PSD.

While much current research involves the study of cutting dynamics, all work is based on time domain simulations, and we did not locate any sources that discussed a frequency domain transfer function for machining processes.

Identifying and Characterizing Elemental Error Terms

We have begun to identify and characterize the elemental error terms that contribute to the net error. The identification of elemental errors will be similar to the traditional error budgeting

methodology, and the results of the literature search are valuable. However, we must also determine characteristic frequency and mean amplitudes of these elemental errors, along with the expected distribution about the mean. These two aspects of the elemental errors are depicted in **Fig. 2**.

We must be able to relate the specific shape of each elemental PSD to our knowledge of that error. For example, since the thermal capacitance of the machine is large, thermal errors will produce relatively low spatial frequency errors. If the machine has encoder feedback, we would expect a positioning error at a spatial frequency of once per revolution of the leadscrew. Each elemental error will have a mean PSD, depicted in **Fig. 2a**, and a distribution about the mean representing the apparently non-repeatable component of this error, depicted in **Fig. 2b**.

We must know the distribution and spread of the PSD about the mean, so we use the appropriate combinatorial rule. We will relate the distribution and spread back to our knowledge of the particular error. For example, the leadscrew positioning error spread will be related to the resolution of the feedback mechanism.

To study the frequency and amplitude content of elemental errors, we measured the positioning error of a moving axis on a T-base lathe. Results are shown in **Fig. 3** in both the spatial domain and frequency domain. Since this machine uses encoders for feedback, we see a very apparent once-per-revolution error of the leadscrew. Note that a machine with scales or laser feedback would not exhibit this error. Surprisingly, we saw a very high frequency error that occurred 320 times every

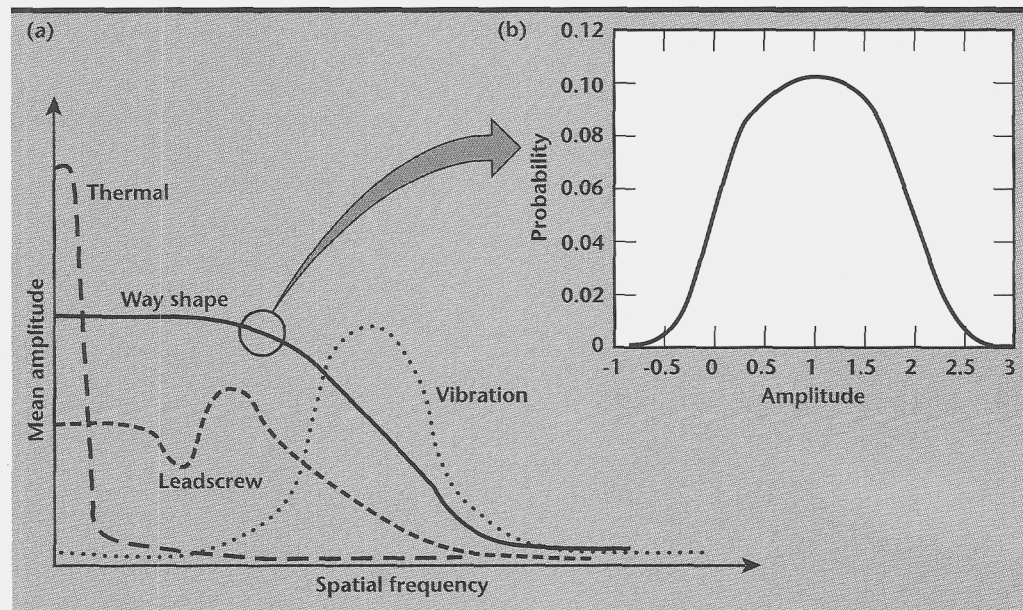


Figure 2. Two aspects of the elemental errors: (a) characteristic frequency and amplitude of four elemental errors, and (b) distributions of the errors about the mean.

revolution of the leadscrew. We are working with Moore, the manufacturer of this machine to identify the source of this error. We believe it is related to the position interpolation procedure of either the machine or the laser measurement system we used to measure the positioning error.

Since the amplitude of this high frequency error is relatively large, a significant amount of aliasing errors occur when the sample rate is not set high enough. From a practical standpoint, it is time-consuming to acquire this finely-spaced data. Conventional measurement procedures take data when the machine is stopped. The machine moves to the new measurement location, stops, and then the measurement is acquired before the machine moves to the next measurement location.

It requires an unreasonable amount of time to acquire data across the full travel of the machine at a sampling rate high enough to avoid aliasing. Furthermore, time-domain filtering cannot be used

to prevent aliasing errors since the machine is not moving at a constant rate. Therefore, we are developing a new measurement procedure that will acquire data on the fly, not requiring the machine to stop at each measurement location. (See the section on Future Work for a description of this measurement procedure.)

On the same T-base lathe, we measured the repeatability of both a positioning error and angular pitch error of a moving axis on a T-base lathe. We found that the angular error non-repeatability was smaller than the resolution of our measuring instrument. This is an important observation which we hope to generalize upon. It may be that certain angular errors can be considered knowns rather than random variables. We also found that the non-repeatable component of the positioning error was much smaller than the repeatable component, and the distribution was near to Gaussian, as shown in Fig. 4. We also measured the repeatability at

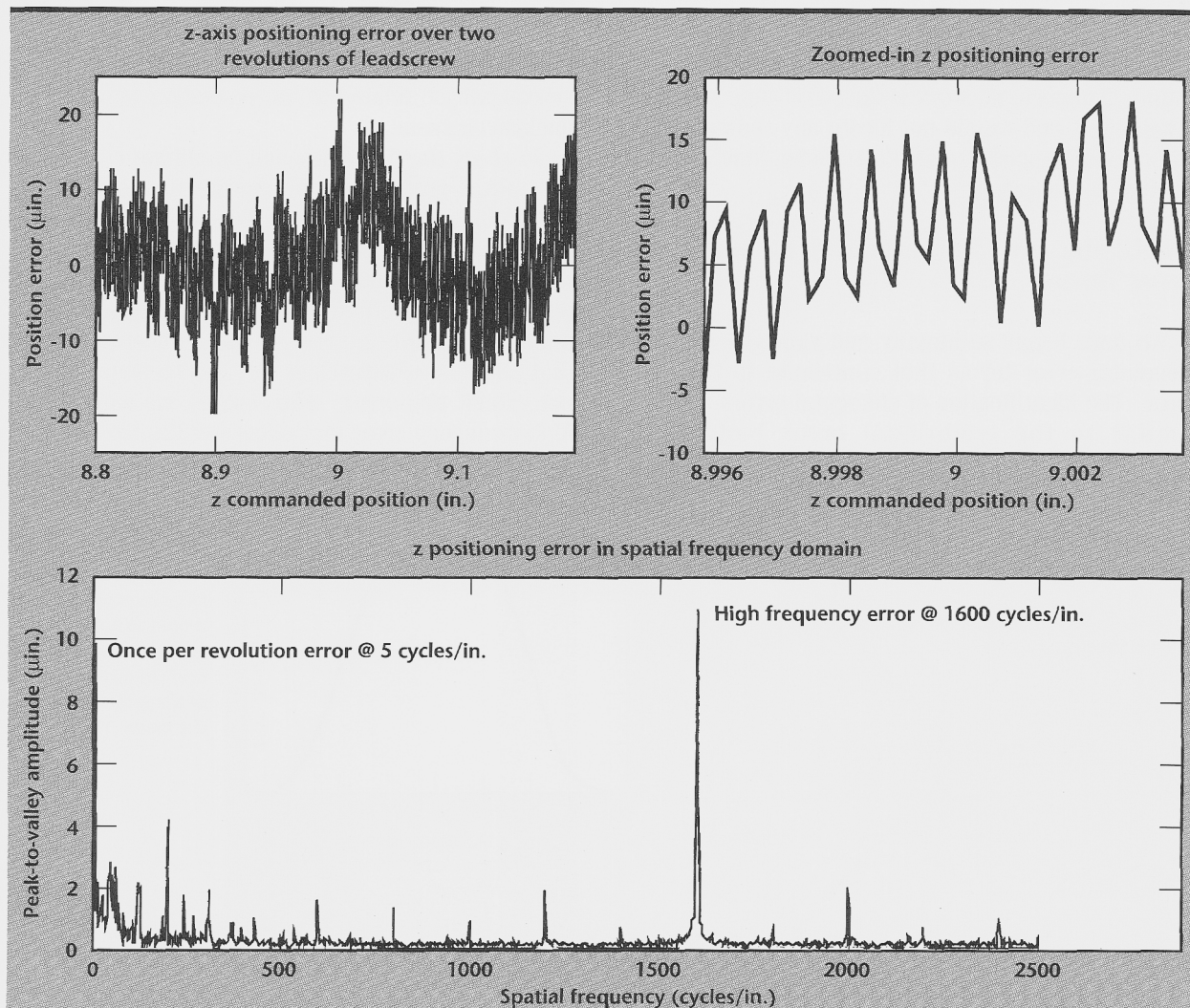


Figure 3. Frequency and amplitude content of an axis positioning error.

different locations along the moving axis and found that the variance is dependent on the position.

Developing a Combinatorial Rule to Sum the Elemental Error Terms

We have developed a combinatorial rule for the addition of elemental PSDs. We have analytically shown that the mean resulting PSD is the sum of the elemental PSDs at each discrete frequency.

However, as a design constraint we are interested in the worst case rather than the mean expected resulting PSD. The worst case scenario would occur if each elemental PSD was simultaneously at a maximum. This could be found by adding the Fourier transforms of the elemental PSDs, and then finding the PSD of the net Fourier transform. When considering sinusoidally varying signals, this would only occur if every elemental error were in phase with the others, and the non-repeatable components of the errors were also at a maximum.

From a statistical standpoint, this scenario is practically impossible. To put practical confidence intervals around the net PSD, it is necessary to determine the distribution and variance of the total PSD as well as the mean PSD.

To determine the net PSD probability distribution function, we considered each elemental PSD to be generated by a sinusoidally varying signal of known amplitude but unknown, uniformly distributed phase. The resulting net PSD probability density function approaches an exponential distribution described by

$$p_{PSD} = \frac{1}{\overline{PSD}} e^{-\frac{PSD}{\overline{PSD}}},$$

$$\overline{PSD} = \sum_i PSD_i,$$

where

\overline{PSD} = mean net PSD,

PSD = net PSD,

p_{PSD} = probability density function of the net PSD, and

PSD_i = i -th elemental PSD.

The probability density function can now be integrated to determine an upper bound on the net PSD given a confidence interval, α . The upper bound is then

$$PSD_{\max} = -\overline{PSD} \ln(1 - \alpha).$$

For a 95% confidence limit, the maximum is approximately three times the mean, and for a 99% confidence limit, the maximum is approximately 4.6 times the mean. This is significantly less than the worst case, when all the errors are in phase. For example, if 25 errors of equal amplitude were summed, the worst case net PSD would be more than eight times larger than the 95% confidence limit, and more than five times larger than the 99% confidence limit.

The spatial frequency domain requirements we have seen are in terms of the power spectral density, so we have concentrated our efforts on determining the distribution of the PSD. However, there may be applications that specify frequency domain errors in terms of the Fourier transform (proportional to the amplitude) rather than the PSD (proportional to the square of the amplitude). We have also determined the probability distribution function for the net Fourier transform, which is directly calculable from the net PSD distribution.

The above results assume that the magnitudes of the elemental PSDs at each frequency are known. In reality, the magnitudes are also random variables with unique distributions at each frequency. This complicates the analysis to the point that it is not feasible to analytically solve for the net PSD distribution.

We have consulted with two professors from the University of California at Berkeley and were advised that in complex situations as this, we should resort to a Monte Carlo simulation. Similar statistical techniques have also been used for tolerance analysis of optical systems.¹⁵ As a tool, we built a Monte Carlo simulation that sums points on the PSD at discrete frequencies. At each frequency, the total

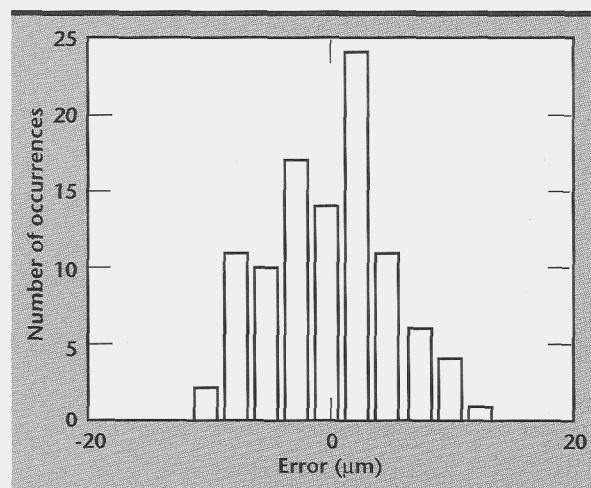


Figure 4. Positioning error repeatability.

error is generated by the sum of sinusoidal elemental errors of known amplitude probability distribution functions and random, uniformly distributed phase shifts. The simulation can be run through 50,000 iterations in less than 30 s.

Figure 5 shows a histogram of the error predictions from 50,000 iterations of the Monte Carlo simulation. In the simulation, 25 errors with amplitude of one and zero variance, and uniformly distributed phases are summed. Since the variance is zero, we can predict the distribution analytically using the exponential distribution.

In the case where the variances of the elemental errors are zero, there is no need to run the Monte Carlo simulation, and the results can be accurately determined using the analytical exponential distribution. This similarity between the histogram and the line shows that the Monte Carlo simulation is working properly.

The Monte Carlo simulation has demonstrated that we must understand the typical distributions of the non-repeatable components of the elemental errors. We found that the particular form of the distribution might not be that critical. For example, if the variance is small in comparison to the mean, the results of the simulation are not significantly different if we assume either uniformly distributed or normally distributed elemental errors. However, as the variance

becomes larger, the elemental distributions become more important.

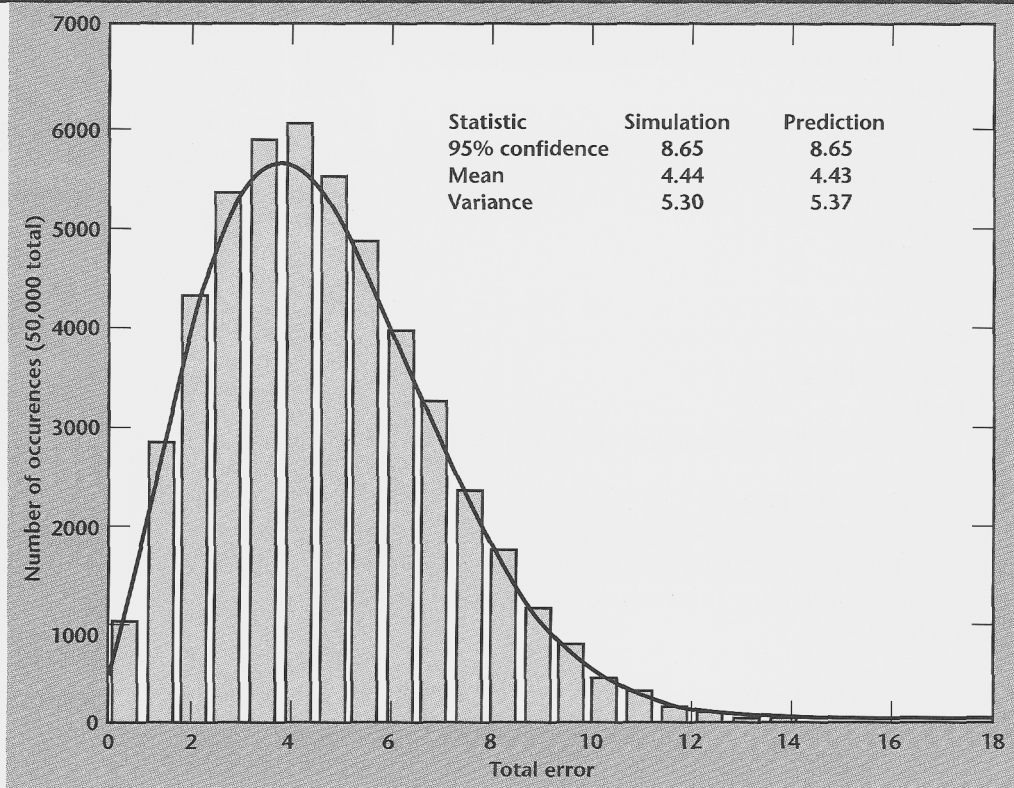
We expect that many of the errors will have small variances in comparison to the mean, or, in other words, the repeatable component of the error will be significantly larger than the non-repeatable component. Therefore, it is critical for us to know the band (minimum to maximum) of the error rather than the exact distribution of the error.

We made a comparison between this new method and the conventional approach at certain spatial frequency bins specified in an error budget for a fly-cutting machine at LLNL.¹⁶ We found that the new method produces similar results for each frequency. This is reassuring since the conventional approach has been shown to produce reasonable predictions. These results are summarized in **Table 1**. The new error budget will have the additional capability of

Table 1. KDP error budget 99.8% confidence limit results.

Frequency bin	Conventional approach	New approach
Roughness	8.70 nm	9.99 nm
Waviness 1	7.45 nm	8.24 nm
Waviness 2	10.54 nm	11.04 nm
Waviness 3	20.95 nm	22.05 nm

Figure 5. Histogram of total error predictions from 50,000 iterations of the Monte Carlo simulation. The plot represents a summation of 25 independent sinusoidal errors with amplitude of one. The line shows the analytical solution.



predicting the full spectrum of errors, rather than single value estimates for the four frequency bins (that is, roughness, waviness 1, waviness 2, and waviness 3).

Developing a Frequency Domain Transfer Function of the Machining Process

The traditional error budget combines the elemental errors of the machining process to predict the motion of the tool in free space. During machining, the tool is in contact with the workpiece. If the machine had no compliance, a one-to-one transfer between the motion of the tool and the resulting surface on the part would occur in a diamond turning process. However, the machine and machining process have some compliance and damping. In actuality, errors that occur at the machine resonance may be amplified by the dynamic process.

Other errors may actually be entirely filtered and not show up on the machined workpiece. We must therefore determine the transfer function between the motion of the tool in free space and the resulting error on the part.

There is much current research in the field of cutting dynamics. However, since the cutting process is highly non-linear, all the research is focused on time-domain simulations of the cutting process. For this project, we don't want to rely on a complex time-domain simulation to produce the transfer function. Instead, our strategy is to make simplifying assumptions that will allow us to develop a frequency-domain transfer function.

We assume that the depths of cut are small, and that the tool will remain in contact with the workpiece for the entire process. We also assume that there are no form errors on the initial part. We also will not be machining at conditions that will excite the resonant modes of the machine, so we are not concerned with the highly non-linear behavior of chatter. We feel that these assumptions are valid for precision machining operations.

We have divided the cutting model development into two phases. The purpose of the first phase is to verify the concept of a frequency-domain approach to representing the machine transfer function using a simple model. The second phase will include a complex turning model, where all the elemental errors will contribute to the final errors on the part. The second phase will be addressed in FY-98 and will be discussed in the next section.

During the first phase, a simple orthogonal cutting model was selected, where only spindle errors and machine dynamics will contribute to the resulting workpiece errors. A cutting model simulation has

been written to produce the transfer function between the tool motion and the resulting errors on the workpiece. Inputs to this simulation include the modal parameters of the machine. We have measured the modal properties of the machine.

A sample transfer function is shown in Fig. 6. Note that this is not the actual transfer function that we will use, because the gain is actually dependent on the amplitude of the error, the mean depth of cut, and the frequency due to non-linearities in the process. Therefore, after we measure the spindle error amplitudes and frequencies, we can generate the true transfer function for this process. During FY-98 we will validate this approach by measuring the spindle errors and machining an actual part. (See the next section for details.)

The output of the transfer function is the motion of the tool while it is in contact with the part. In combination with the feed-rates of the axes, we can generate the amplitude and frequency content of the resulting errors on the part in the direction of the tool motion. However, this does not predict the errors during a turning process "across the lay," that is, perpendicular to the direction of the tool. Since the errors in both directions are relevant to workpiece specifications, we are also developing a procedure to determine the amplitude and frequency content of the residual errors perpendicular to the path of a tool during a turning process.

To determine the amplitude and frequency content of the tool motion, we use the output from the transfer function which predicts the frequency and amplitude content of the tool motion while it is in contact with the part. Next, the tool motion is sampled by the reciprocal of the feed-rate, where the feed-rate units are distance per revolution and the reciprocal units are revolutions (or cycles) per distance. Note that the units of the spatial-domain frequency (cycles per

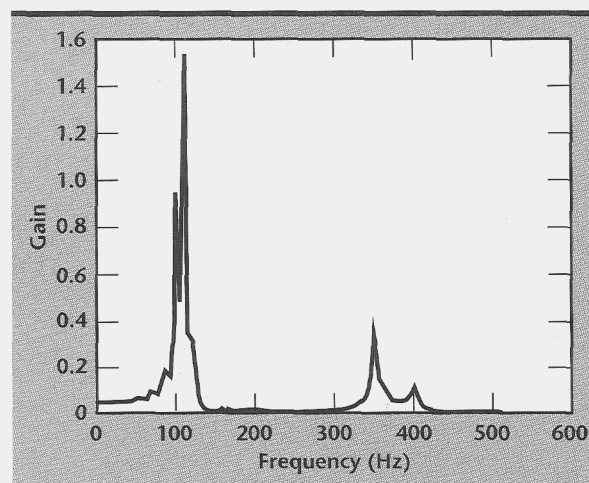


Figure 6. Machining process transfer function for Phase 1.

distance) are the equivalent to time-domain frequency units of Hz (cycles per second).

When the frequency of the tool motion is less than one half the sampling frequency, the sampling procedure is fairly straightforward. Since sampling is a multiplication process in the time domain, this is equivalent to a convolution process in the frequency domain. However, when the frequency of the tool motion is greater than one half the sampling frequency, unavoidable aliasing occurs. We must then determine the apparent frequency and amplitude content of the aliased signal.

For example, if the frequency of the tool motion is an integer of the sampling rate, the sampled signal will appear to have only a DC off-set. (See Fig. 7 for a relationship between the frequency of the error and the apparent frequency after aliasing.) During FY-98 we will further investigate this relationship.

The nominal surface finish generated when the machine has no errors has some amplitude and frequency content, caused by the shape of the tool. For a tool with a flat profile, the nominal surface finish would be flat; however, most tools have a round profile, creating surface finish errors at spatial frequencies of once per feed-rate, and higher harmonics. Previous work has investigated the nominal surface finish and, based on geometry, the nominal peak-to-valley surface error across the lay is

$$PV = \frac{f^2}{8R}$$

f	=	feed-rate (distance/revolution)
R	=	tool radius (distance)
PV	=	peak-to-valley error (distance).

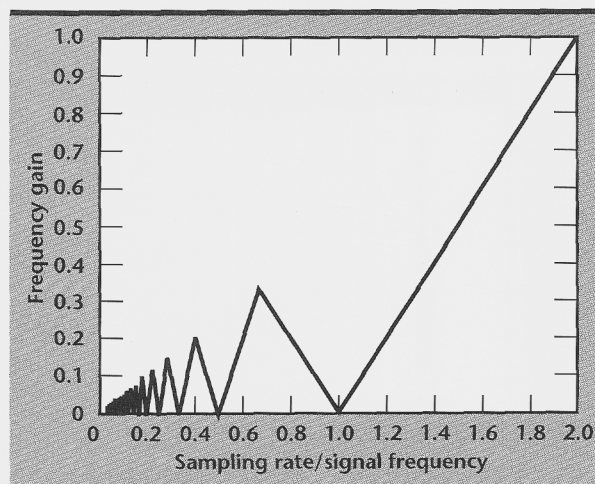


Figure 7. Apparent frequency gain after aliasing.

We have started to investigate how the nominal frequency content and the error frequency content add to produce the final errors on the part. Figure 8 shows the nominal surface finish and the surface finish when the tool motion is given a sinusoidal error at a single frequency. The error motion has a filtering effect on the surface finish. These surface finishes are shown in the frequency domain in Fig. 9.

During FY-98, we plan to show that the frequency content of the actual surface can be attained by appropriately adding the aliased frequency content of the error motion and the frequency content of the nominal surface. This will be discussed in more detail in the following section.

Future Work

Identifying and Characterizing Elemental Error Terms

In actual usage of the error budget, it is not possible to measure all the errors on a new machine before the machine has been built. Therefore we need a procedure to predict the frequency and amplitude content of the elemental errors from the physical properties that create the error.

To develop this procedure, we will fully characterize the frequency and amplitude content of many of the significant elemental errors that contribute to the net error on a T-base lathe. We will relate the form of the elemental error to physical sources that create the error. We will create generalizations that will provide a methodology for predicting the frequency and amplitude contents of the elemental errors to the physical sources.

We will develop a new measurement capability, a high speed data acquisition system that triggers off position so our measurement data is evenly spaced in position. This is necessary so our spatial frequency domain calculations based on digital Fourier transform (dft) techniques are correct. To accomplish this, a laser interferometer will measure position in line with the measured error, and we will trigger off the laser interferometer. We have purchased the appropriate hardware in FY-97 and will design and implement this system in FY-98.

Developing a Combinatorial Rule to Sum the Elemental Error Terms

This task was completed in FY-97. The procedure will be summarized and incorporated into the full error budget procedure.

Developing a Frequency-Domain Transfer Function of the Machining Process

We have divided this task into two phases. The purpose of the first phase is to verify the concept of a frequency-domain approach to representing the machine transfer function using a simple model.

During FY-97, a time-domain cutting simulation was written to produce the frequency-domain transfer function (see previous section).

In FY-98, we will measure the spindle error motion that contributes to the error on the machined part. This error motion will be input into the time-domain simulation to produce the frequency-domain transfer function. From the transfer function and the motion of the tool in free space, we will predict the resulting frequency and amplitude content of the surface finish of an orthogonally turned part. We will then machine an actual part, measure the surface finish, and compare the prediction to the measurement.

The second phase will include a complex turning model, where all the elemental errors will contribute to the final errors on the part. We have contracted Northwestern University to establish a methodology for determining frequency-domain transfer functions of cutting processes during machining.

Northwestern's tasks include developing a generalized methodology to determine the frequency-domain transfer function, and one case study that applies this methodology to one particular machining operation. The machining process used for verification of the model will be a turning procedure of a hemispherical part. Northwestern will provide a transfer function along the direction of the tool path.

We will perform this machining operation and characterize and sum the elemental errors during the machining process to determine the frequency content of the tool motion in free space. Using the transfer function developed by Northwestern, we will predict the frequency and amplitude content of the residual errors on the machined part. We will

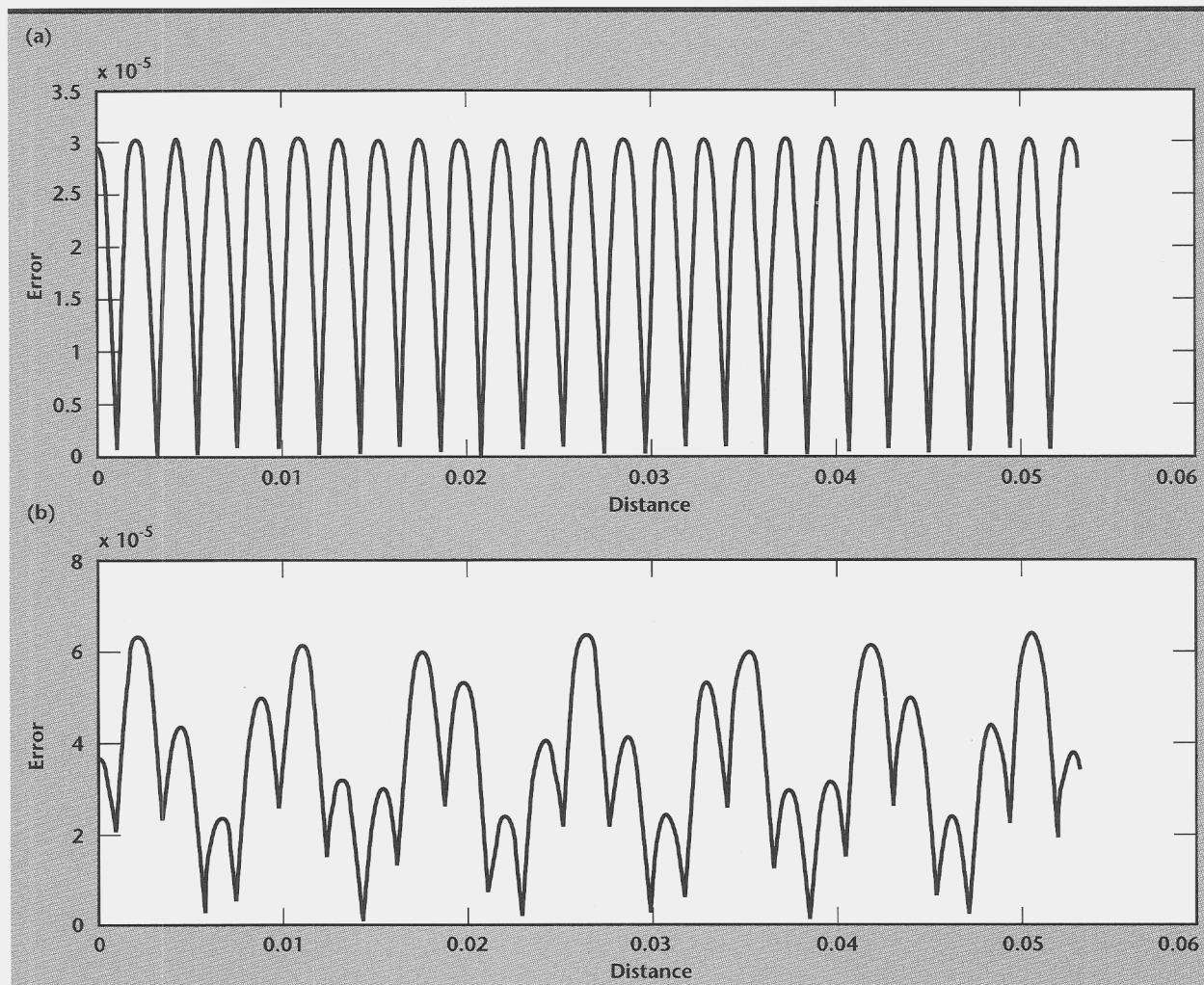


Figure 8. Nominal surface finish (a) and actual surface finish (b) of turned part perpendicular to tool motion.

measure the frequency content of the surface finish of the machined part and the measurements will be compared to the prediction.

Note that the machine that we will use to create the hemispherical testpiece will be the same machine that will be fully characterized to study the elemental error terms.

We also need to predict the frequency and error content of the residual errors perpendicular to the motion of the tool. During FY-98, we plan to show that the frequency content of the actual surface can be attained by appropriately adding the aliased frequency content of the error motion and the frequency content of the nominal surface (See previous section for more details). We have written simulation that creates the surface errors on a part given the tool geometry, feed-rate, and error motion of the

tool. Our hypothesis is that the resulting errors on the part can be determined by appropriately filtering the simple addition of the aliased frequency content of the error motion and the frequency content of the nominal surface. Using the simulation, we will develop this relationship. We will then predict the surface finish of the machined part perpendicular to the tool motion and compare the prediction to measured values off the machined part.

Integration

The last effort will be to put each task in the error budget together into a usable procedure. This includes procedures to 1) identify and predict the frequency and amplitude characteristics of the elemental errors; 2) sum elemental errors to predict

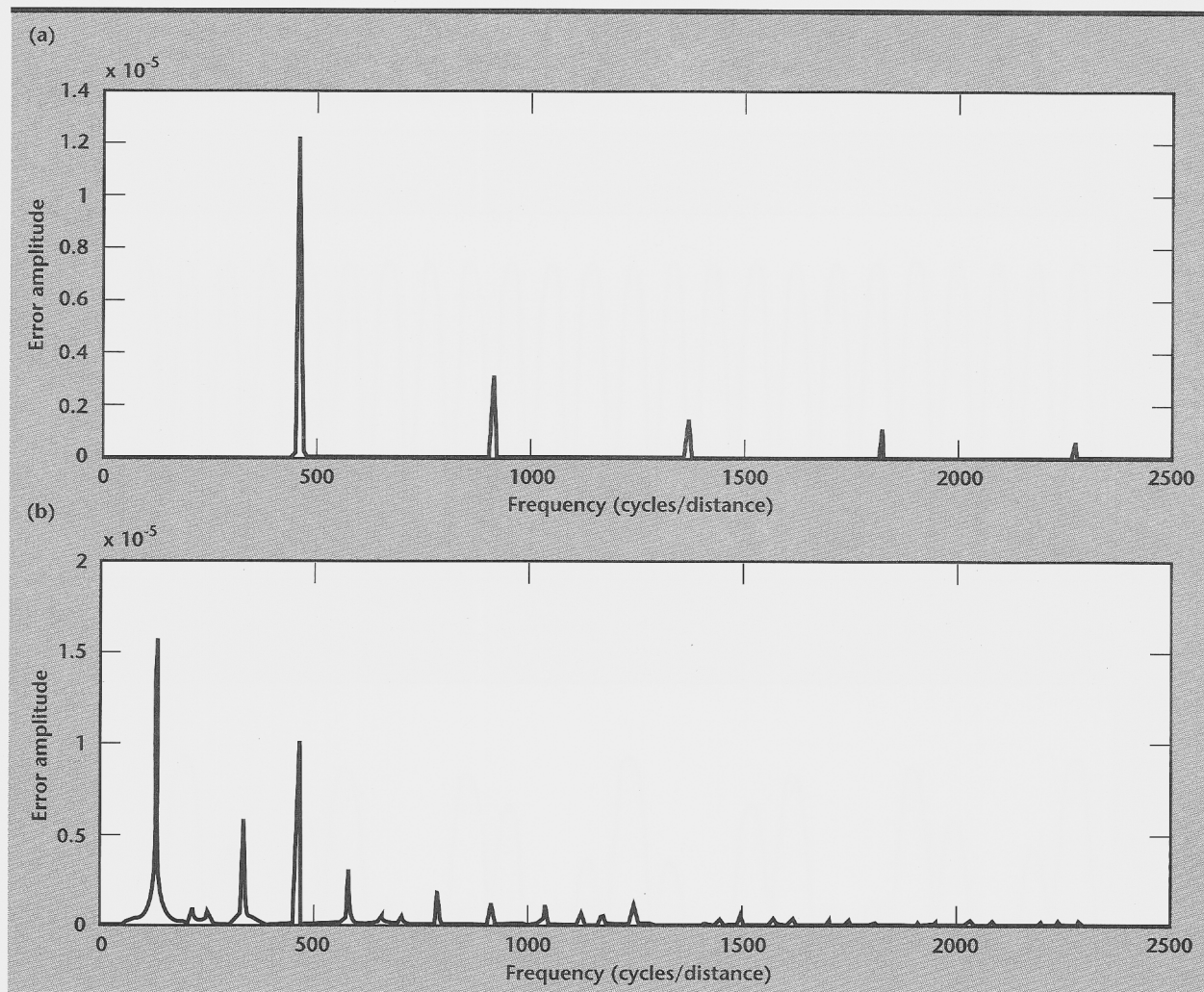



Figure 9. Frequency content of the nominal surface finish (a) and actual surface finish (b) of turned part perpendicular to tool motion.

the frequency and amplitude content of the tool motion in free space; 3) develop a frequency-domain transfer function between the motion of the tool in free space and the motion of the tool while it is in contact with the part during machining; 4) predict the frequency and amplitude content of the surface finish of the part along the direction of the tool; and 5) predict the frequency and amplitude content of the surface finish of a part perpendicular to the direction of the tool.

References

1. Aikens, D. M. (1995), "The origin and evolution of the optics specifications for the National Ignition Facility," *Optical Manufacturing and Testing*, V. J. Doherty and H. Philip Stahl, Eds., SPIE Vol. 2536, pp. 2-12.
2. Church, E. L. and P. Z. Takacs (1994), "Specification of the Figure and Finish of EUV Mirrors in Terms of Performance Requirements," *OSA Proceedings on Extreme Ultraviolet Lithography*, F. Zernike and D. T. Atwood, Eds., Vol. 23, pp. 77-82.
3. Lawrence Livermore National Laboratory, Livermore, CA, UCRL-52000-95-4 (1995), "Creating Microsphere Targets for Inertial Confinement Fusion Experiments," pp. 1-9.
4. Donaldson, R. R. (1980), "'Error Budgets,' in Machine Tool Accuracy," *Technology of Machine Tools: A Survey of the State of the Art by the Machine Tool Task Force*, R. Hocken, Ed., Vol. 5 (9).
5. Dorndorf, U., V. Kiridena, and P. Ferreira (1994), "Optimal Budgeting of Quasistatic Machine Tool Errors," *Journal of Engineering for Industry, Transactions of the ASME*, Vol. 116 (1), pp. 42-52.
6. Gee, A. (1994), "'Error-Budgeting' for High Performance Positioning in Ultra-Precision Manufacture," *IEE Colloquium (Digest) IEE Computing and Control Division Colloquium on Precision Motion Control in Robotics and Machine Drives*, November, 226, pp. 3/1-3.
7. Slocum, A. H. (1992), *Precision Machine Design*, Prentice Hall, Princeton, NJ.
8. Thompson, D. C. (1989), "The Design of an Ultra-Precision CNC Measuring Machine," *39th CIRP General Assembly, Trondheim, Norway*, August.
9. Treib, T. (1987), "Error Budgeting—Applied to the Calculation and Optimization of the Volumetric Error Field of Multiaxis Subsystems," *Annals of the CIRP*, Vol. 36 (1), pp. 365-368.
10. Zakovorotny, V., I. Ladnik, and S. Dhande (1995), "A Method for Characterization of Machine-Tools Dynamic Parameters for Diagnostic Purposes," *Journal of Materials Processing Technology*, Vol. 53, pp. 588-600.
11. Shen, Y., and N. Duffie (1993), "Comparison of Combinatorial Rules for Machine Error Budgets," *CIRP Annals*, Vol. 42 (1), pp. 619-622.
12. Shin, Y., and Y. Wei (1992), "A Statistical Analysis of Positional Errors of a Multiaxis Machine Tool," *Precision Engineering*, Vol. 14 (3), pp. 139-146.
13. Spotts, M. (1975), "The Combination of Uniform Probability Curves in Engineering," *ASME Design Engineering Technical Conference*, Washington, DC, September.
14. Bendat, Piersol, J. M. Elson, and J. M. Bennett (1995), "Calculation of the power spectral density from surface profile data," *Applied Optics*, 34 (1), pp. 201-208.
15. Wilkinson, E., J. Green, and D. Sahnou (1994), "Tolerance analysis of the Far Ultraviolet Spectroscopic Explorer (FUSE): a statistical approach," *Proceedings of SPIE—The International Society for Optical Engineering X-Ray and Ultraviolet Spectroscopy and Polarimetry, San Diego, CA*, July, Vol. 2283, pp. 261-264.
16. Moore Tool Company, Inc. (1995), "Diamond Turning Machine for KDP Crystal Manufacturing," *Conceptual Design Report*, November. 

icro-Drilling of ICF Capsules

Steven A. Jensen

*Manufacturing and Materials Engineering Division
Mechanical Engineering*

We have investigated the commercial capability of micro-drilling in terms of the current limits to precision, quality, and aspect ratios attainable. The motivation behind this study is to determine the feasibility of drilling a small hole in the National Ignition Facility fusion capsules, suitable for filling with the intended fuel mixture. The challenge of accomplishing this task is that the hole to be drilled must have a very high aspect ratio (up to 100 to 1, or beyond), and be drilled in such a manner that it does not become a major structural defect or perturbation to the overall capsule. From the information available, it does seem feasible to create micro-holes suitable for filling. Based on preliminary investigations, however, it does not seem likely that a commercial company will be able to produce these holes.

Introduction

The National Ignition Facility (NIF) at Lawrence Livermore National Laboratory (LLNL) will require spherical shell targets about 2 mm in diameter, with ablator shell thickness between 100 and 150 μm . These targets will be filled with a deuterium-tritium (DT) fuel mixture, and ultimately struck from all directions, simultaneously and uniformly, by sufficient radiant energy to vaporize or ablate the outer capsule shell, which will then expand in a rocket-like blow-off. This rapid expansion of the ablator drives the inner portion of the capsule inward, compressing and heating the DT fuel contained inside. By the end of the implosion, the fuel core reaches a high enough density and temperature to initiate nuclear fusion.

The shape and symmetry of the compressed fuel during implosion is critical to capsule performance. Irregular or non-uniform compression of the DT fuel could create conditions that fall short of complete ignition. The uniformity and smoothness of the ablator shell plays a significant role in the proper compression of the DT fuel. For this purpose, the capsules need to be made with as few structural defects or surface perturbations as possible. Currently the required surface roughness for these capsules is on the order of 10 nm rms, or less.

Progress

We have studied the micro-drilling process in terms of current limits to processing quality and aspect ratios for fusion capsules.

Capsule Fabrication and Design

There are three approaches being pursued for an ablator capsule. The first approach, and most direct, is to machine two hemi-shells from bulk material and bond them together. The second approach involves coating a hollow mandrel (possibly in some chemical vapor deposition (CVD) process, or by sputtering), and then drilling a small hole in the capsule, suitable for filling. Once filled, this hole would be plugged or welded shut. The third, and most current, method for capsule fabrication involves sputtering a hollow polymer mandrel (polystyrene 3 to 6 μm thick), which is then diffusion-filled.

Several materials were originally chosen as candidates for the ablator shell, among which were B, B_4C , B_9C , CH, and doped Be. Doped Be was eventually chosen because it offers advantages in lower density, better hydrodynamic stability, reduced drive temperatures, faster sputtering rates, and overall strength characteristics.¹ The hollow mandrels are sputter-coated with the doped Be using

three magnetron sputter guns and a piezoelectric-driven bounce pan, which is used to help ensure a uniform coating.

The bounce pan is electrically isolated, so that, if desired, a voltage bias can be applied. By applying a voltage bias, the morphology and grain structure of the deposited Be can be altered. This becomes important when attempting to diffusion-fill the capsules. Ideally, the capsules would be diffusion-filled at or near room temperature; however, this requires that the porosity of the capsule be near 10%. The downside to this is that as the porosity increases, so does the over all surface roughness, and a porosity of 10% does not meet the surface roughness requirements of less than 10 nm rms. By applying a voltage bias, the morphology of the deposited Be becomes more compact and less porous, which leads to better surface roughness values.

However, current efforts to diffusion-fill these less porous capsules have not been successful. Attempts have been made at using elevated temperatures to aid the diffusion-filling process, but these elevated temperatures tend to melt the inner polystyrene mandrel. Furthermore, even when using a voltage bias, current efforts have not produced a capsule having the required surface roughness of 10 nm rms or less (50 nm rms has been the best). This suggests that even in the event that the capsules can be diffusion-filled, some type of post-processing, such as micro-polishing, may be required to improve surface finish of the deposited films.

Micro-Drilling of Capsules

The advantages to using a micro-hole as a means to fill the capsules are as follows:

- 1) It will be much easier to attain the required surface roughness if the grain morphology is more tightly packed (hence non-porous). Currently, capsules are sputter-coated to be somewhat porous so they can eventually be diffusion-filled. This limits the quality of the surface roughness attainable. If there existed a small hole suitable for filling, the ablator shell would not need to be porous at all.
- 2) Porous capsules that are capable of being diffusion-filled are just as capable of leaking. To prevent this, the capsules are over-filled and then cryogenically handled up until they are positioned at the center of the target chamber. If a suitable micro-hole could be drilled, filled, and then sealed in a non-porous capsule such that there were no leaking, the need for cryogenic handling from the time of fill would be

eliminated. This would ultimately add flexibility to the process and would represent a significant saving in cost.

We looked at several methods of creating micro-holes. One method is to mechanically drill the holes using a very small drill bit. The drawback to this method is that mechanical drill bits are limited in size to, at absolute best, 12 to 15 μm in diameter. Furthermore, mechanically drilled holes of this size are limited to, at best, a 5 to 1 aspect ratio.

Another method would be to electroplate around a post made of polymethyl methacrylate, or some other polymer that would eventually be dissolved away, leaving a hole. This method does allow for very straight and small holes having a high aspect ratio and good quality, but electroplating Be is not currently done.

A third method would be to use a chemical etching process to create the hole, but, as with mechanical drilling, the aspect ratios would be limited.

Still another method, and relatively new, would be to use supersonic waves. This technique, which is still in the research and development stages in Japan, uses a small hard metal tool (about 4 μm in diameter), and some small diamond powder abrasive (0.25 μm grit size), in conjunction with supersonic waves, to chisel away small fragments of material. It is not yet known if this technique is suitable for metals, since it has been tested only on glasses and ceramics.

Finally, the holes could be created using a laser drilling process. The information in this report will focus on the issues related to the laser drilling approach to creating micro-holes. More specifically, it will define the current limitations to commercially drilled holes and outline possible solutions by which work at LLNL can possibly overcome these limitations.

Commercial Vendors

To determine the status of the commercially available technology for laser drilling, several companies specializing in small hole technology were contacted and consulted on holes that they were able to produce. Although eight companies were contacted, only three claimed to have the ability to commercially produce holes less than 5 μm in diameter, having relatively high aspect ratios. Those companies are Resonetics (New Hampshire), Lenox Lasers (Maryland), and Oxford Lasers (Massachusetts).

Two of these vendors (Resonetics and Lenox Lasers) were chosen to drill holes in samples for evaluation purposes. SEM photographs of a few sample holes drilled by these companies, are shown in Fig. 1.

Challenges Associated with Micro-Drilling

There are some significant challenges to be resolved using the laser drilling approach. First of all, the laser technology for drilling very small precision holes, on the order of 5 μm in diameter or less, is still in its infancy. Most commercial vendors do not have the equipment or expertise to drill holes this small. Work is currently being done in this area, including at LLNL. However, this work is not yet able to consistently produce micro-holes in a conventional manufacturing setting.

The first fundamental limitation to producing very small micro-holes is the diffraction limit of the optical system. The governing equation for the attainable spot size diameter of the laser beam is given by:

$$\text{dia} = 1.27 \cdot f\# \cdot \lambda$$

where $f\#$ is the f-number, defined as the focal length divided by the diameter of the optic (L/D), and λ is the wavelength of the laser beam. For a given wavelength the only way to reduce the spot size is to

reduce the f-number. Optics having a low f-number have high resolution and produce small spot sizes, but at the expense of having a limited range of material penetration. Conversely, optics having a larger f-number are able to penetrate to higher depths, but at the expense of a limited hole size diameter. Having a laser with a very short wavelength becomes critical to producing very small holes having a high aspect ratio.

In the commercial field, excimer lasers are most often used to produce small holes. These lasers typically have a wavelength of 247 nm. Realistically, this needs to be smaller if holes on the order of 1 to 2 μm in diameter are to be drilled.

The other two major problems associated with drilling small precision holes, as they relate to the NIF capsules, are the taper angles associated with high aspect ratio holes, and thermal damage to the substrate. These key limitations are outlined below.

Taper Angle. Because the ablator shell of the capsule is between 100 and 150 μm thick, and the desired holes are to be less than 5 μm (ideally 1 to 2 μm) in diameter, the holes must have a very high aspect ratio (up to 100 to 1). Drilling high-aspect

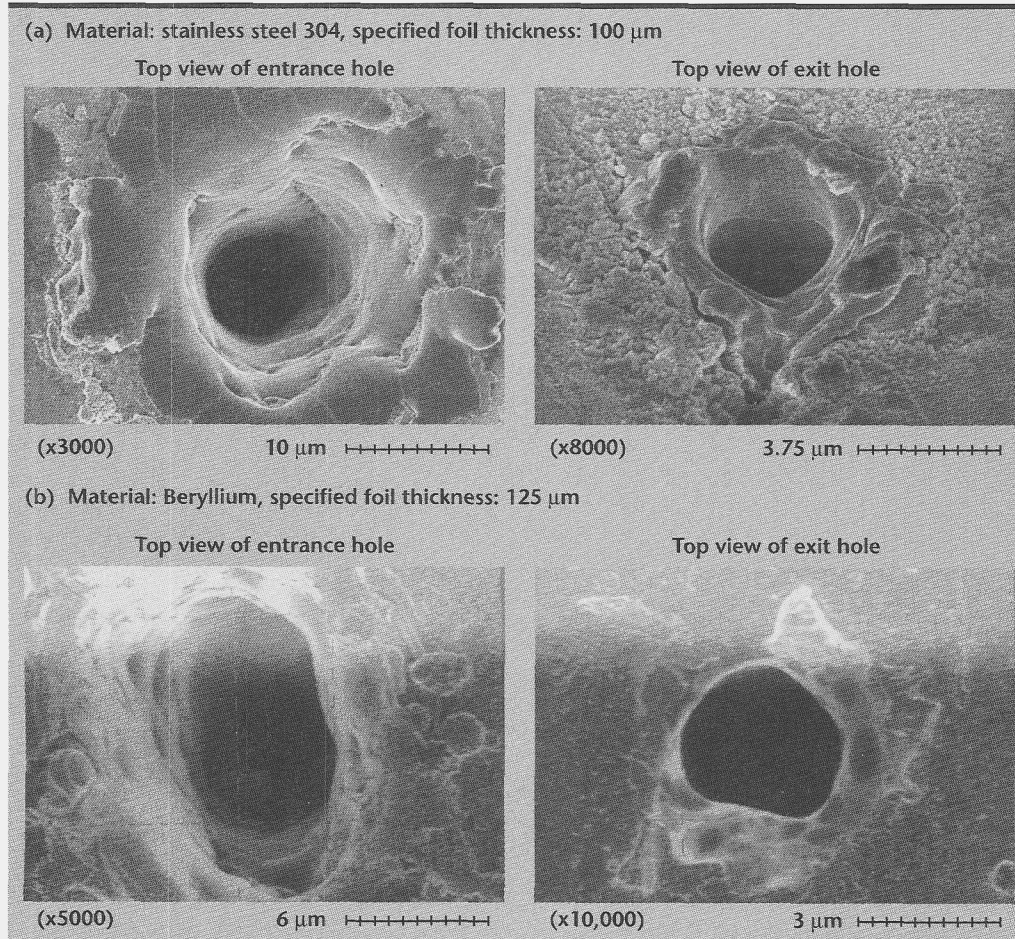


Figure 1. SEM photographs of holes drilled by commercial vendors, (a) Lenox Lasers, and (b) Resonetics.

ratio holes in and of itself is difficult, but drilling them straight without any taper or angular deviance is a much tougher task. Most laser drilling techniques produce holes which have a slight nominal taper angle. (In actuality the holes have a cross-sectional appearance similar to that of an inverted wine bottle.) Commercial taper angles typically range between 4° or 5° , at best, and 10° or 12° for relatively clean holes having minimal thermal damage. A schematic showing this taper angle is depicted in **Fig. 2**.

Because of this taper angle, the entrance diameter will be larger than the exit diameter, and can become quite significant for high aspect ratio holes. Assuming an exit hole diameter of $1\text{ }\mu\text{m}$ and an ablator shell thickness of $100\text{ }\mu\text{m}$, the entrance hole diameter would range between approximately $8\text{ }\mu\text{m}$, at best, and as much as $22\text{ }\mu\text{m}$. A hole entrance diameter of this size starts to become a major structural perturbation in the capsule shell.

The generated taper comes as a result of a combination of effects. Some researchers have attributed the taper to the spatial intensity distribution of the focused laser beam (shaped similar to Gaussian distribution) and light reflected off the side walls. Resonetics recently finished a project funded by NASA, where they attempted to make a particular excimer laser beam 10 times more coherent than previously possible. It was anticipated that this would reduce the taper angle, creating a straighter hole.

However, the results seemed to indicate that it had little or no effect on the taper angle. Since then, they speculate that it is more of a function of thermal heating and diffusivity into the surrounding lattice structure, and the direction and flow of the melt products. This view is also shared in part by other researchers at LLNL. This is best described in the following section on thermal effects.

Generally speaking, micro-holes are created by either evaporative or melt expulsion, or brittle materials spallation. Which one of these mechanisms dominates the process depends on the material and the processing parameters used. Overall, these

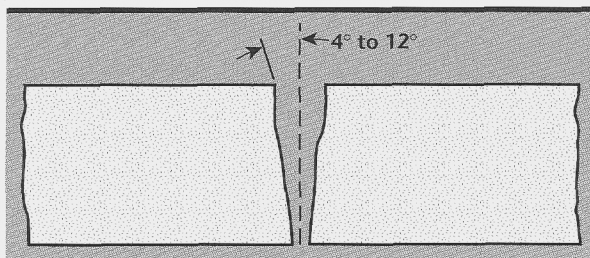


Figure 2. Taper angle of typical commercial laser-drilled hole.

mechanisms determine the geometrical shape of the resulting hole, and the extension and geometry of the heat and mechanically affected zones (**Fig. 3**).

Figure 3 represents a typical view of the laser drilling process in a metallic substrate. Evaporative expulsion takes place when surface material is superheated to the gas or plasma state. This type of drilling is referred to as true thermal ablation. The amount of thermally ablated material is typically very small for most commercial drilling operations, due to longer pulse lengths (nanosecond regime or longer).²⁻⁴

The larger part of the pulse energy is used to heat up the material until ablation starts at the end of the pulse. As a consequence, most of the beam energy is lost, due to heat conduction into the bulk material. Material that is at a temperature just below the superheated gaseous state remains molten. The molten material is expelled due to the ablation and plasma pressure. This has adverse effects on the geometry of the hole. The larger entrance hole is more than likely attributed to erosion of the side walls from the expulsion of melt products.

The SEM photographs in **Fig. 1** show samples of entrance and exit holes drilled in stainless steel and beryllium.

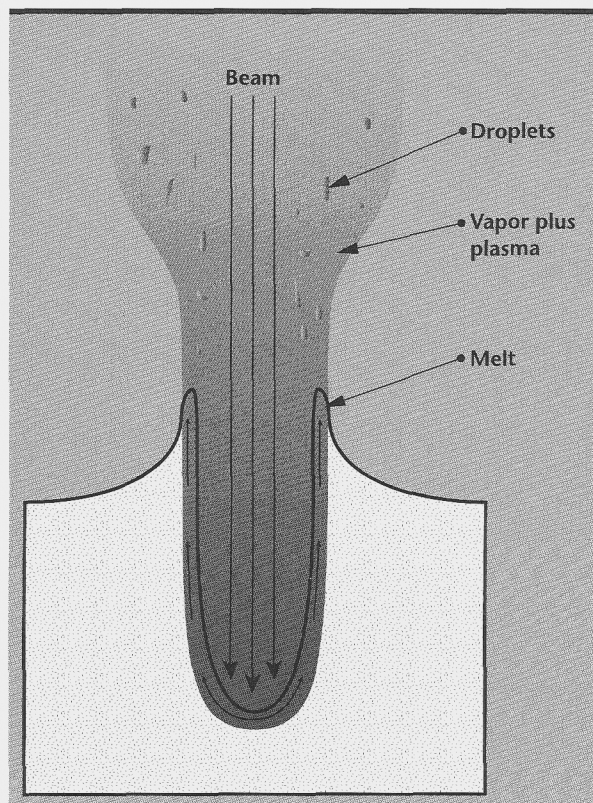


Figure 3. Schematic of typical view of the laser drilling process in a metallic substrate.

For the particular application of drilling holes in an ablator capsule, the taper will need to be reduced to angles ideally below 3° to 4° , which, for a $1\text{-}\mu\text{m}$ exit hole in a $100\text{-}\mu\text{m}$ -thick substrate would give an entrance hole diameter ranging between approximately $4\text{ }\mu\text{m}$ and $8\text{ }\mu\text{m}$.

Thermal Effects. The majority of all laser-drilled micro-holes, commercial or non-commercial, are made by literally burning a hole through the metallic substrate. The hole is mostly created by the expulsion of molten material, which leads to the formation of dross, thermal re-cast layers, and thermal cracking. Equally present, but not always visible, is the formation of dislocations, slip planes, and residual stresses. All of these adversely affect the overall integrity of the capsule and could lead to conditions that fall short of complete ignition.

The SEM photographs in Fig. 4 show some extreme cases of thermal damage associated with laser drilling holes in stainless steel foil samples. Stainless steel is one of the worst materials to laser-drill, due to its inhomogeneity, which produces more than average amounts of dross and re-melt. Holes drilled in highly homogenous materials, and having a relatively small grain size, produce cleaner holes with less dross and re-melt. Such materials include tungsten, tantalum, molybdenum, and beryllium.

Laser Drilling of ICF Capsules

In view of the problems associated with laser-drilling, a "best effort" approach was taken to drill holes in some actual sample target capsules using commercial capabilities. The idea was to try and drill as small a hole as was commercially available, while minimizing the thermal effects by using as short a laser pulse length as possible.

Target capsules approximately $500\text{ }\mu\text{m}$ in diameter with a wall thickness of about $17\text{ }\mu\text{m}$ were sent from

LLNL to Resonetics. Three holes were drilled in three separate targets using an excimer laser having a wavelength of 193 nm . The optical set-up had a recorded diffraction limit of $6\text{ }\mu\text{m}$. The other important parameters were as follows: laser energy, 550 mJ ; demagnification, 16.5 ; and measured fluence, 43 J/cm^2 . SEM photographs of two of the drilled holes are shown in Fig. 5.

The photographs do show some thermal re-melt layers, but, overall, the heat-affected zone is not overly large in comparison to the hole diameter. These photographs also show the columnar and porous structure of the sputtered, beryllium surface of the targets. Although these targets had a wall thickness of only $17\text{ }\mu\text{m}$, far less than what will eventually be needed, the holes do show some promising signs of being used as a filling orifice. If a laser set-up capable of femtosecond pulses were used to drill the holes, and if the diffraction limit of the laser set-up were lowered to 2 to $3\text{ }\mu\text{m}$, the holes would be much cleaner and smaller, as described in following section.

Femtosecond Laser Ablation

As stated earlier, the creation of holes in metallic substrates is done by either melt expulsion or evaporative expulsion, also known as true thermal ablation. In a true thermal ablative process, the material is converted from a solid state to a vapor or plasma state very rapidly. This then either evaporates or, ideally, would be extracted through the use of a vacuum.

True thermal ablative processes require very short pulses of energy, on the order of femtoseconds. Theoretically, when the laser energy interacts with a material, it is first deposited into the free electrons, which rapidly cool by transferring this energy to the lattice structure. The cooling of

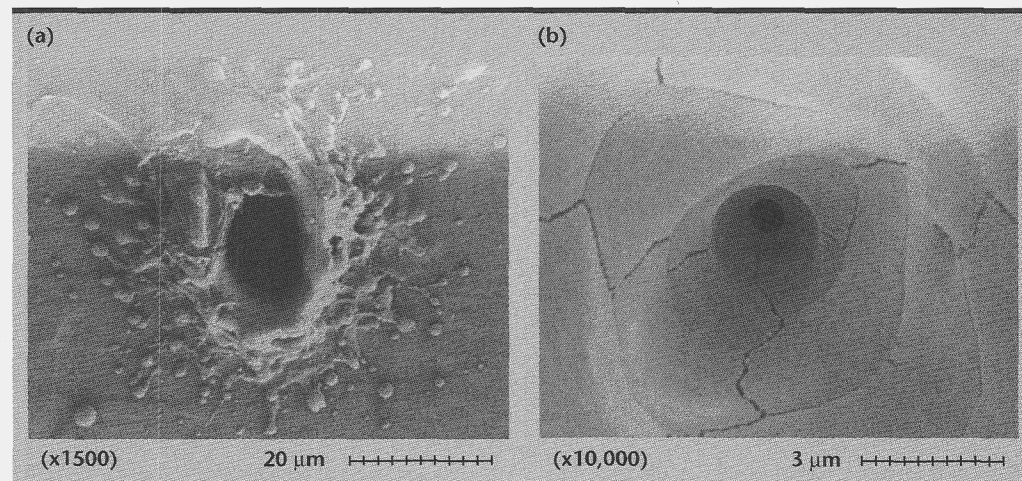


Figure 4. SEM photographs showing extreme cases of thermal damage associated with laser-drilled holes in stainless steel: (a) top view of entrance hole, showing dross and re-melt; and (b) inside view, showing thermal cracking.

the electrons and transfer of energy happens on the order of 1 ps, which is much longer than the laser pulse duration (when operating in the femtosecond regime).

If the energy transferred is above the evaporation threshold for the particular material, then the lattice material is converted from the solid phase to the vapor and plasma phase. This happens so rapidly that thermal diffusion into the target is negligible, so there is very little heating of the surrounding areas.⁴⁻⁸ Therefore, there is virtually no re-melt, thermal cracking, or generated dross, because of the absence of the liquid phase.

The SEM photograph in **Fig. 6** shows a hole drilled in 100- μm -thick steel, using a short pulse laser (that is, a femtosecond laser).⁷ Although the hole is quite large in diameter, it does show the advantages of using a short pulse laser to minimize thermal damage to the substrate. The pulse lengths used to drill the hole were on the order of 200 fs.

The use of femtosecond technology is relatively new, and commercial vendors typically do not have lasers capable of generating these pulse lengths. Commercial vendors typically have excimer-type lasers, which can produce pulse lengths as short as 20 ns, but usually no shorter. In fact, the shortest

pulse length used to drill the holes in the previously shown SEM photos was approximately 25 ns.

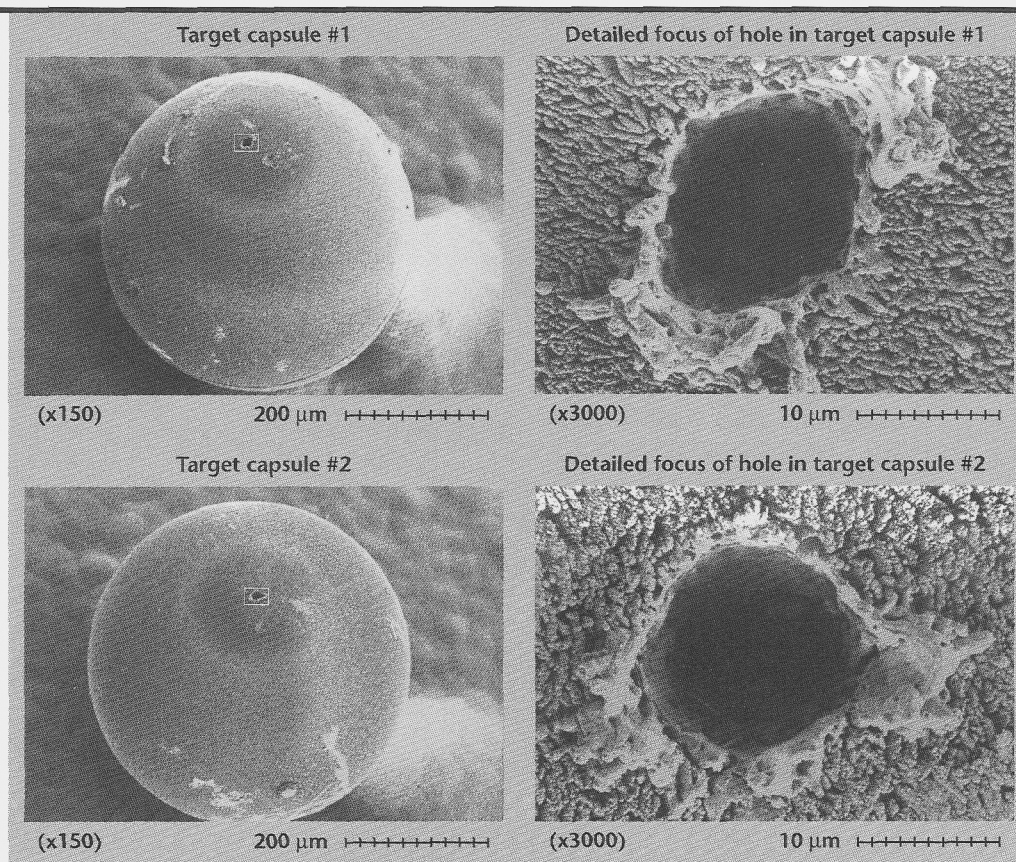
Currently, micro-holes drilled using femtosecond technology are limited to research and development facilities. There are several femtosecond lasers at LLNL.

Micro-holes drilled using pulse lengths in the nanosecond regime more than likely will not produce high enough integrity holes to meet the stringent NIF requirements for the target capsules. Laser pulses on the order of nanoseconds are too long, resulting in significant heat transfer to the surrounding lattice structure, causing re-melt, and thermal cracking of the material, as evidenced in the SEM photographs.

It should be pointed out that, even using a femtosecond pulse laser, there are still the issues of aspect ratio and taper angle. For the most part, only thermal effects will be eliminated. Preliminary studies have shown that even femtosecond pulsed lasers create a taper angle, and that it is not much better than the taper angles associated with longer pulse lasers.

New research suggests that using a flat-top beam will help reduce this, but it is not known just how much of an effect it will have on very small holes

Figure 5. SEM photographs of laser-drilled holes in two sample target capsules, (a) and (b).



with a high aspect ratio. The ablation process, when using a femtosecond laser, is mostly dependent on the intensity of the beam and the material properties. During drilling, an energy field is created in the walls and results in current conduction. This leads to a loss of energy through the side walls. The smaller and deeper the hole is, the more energy is lost through the side walls. When the intensity of energy gets too low, stalling occurs where no material is ablated.

Efforts are being made at LLNL to drill holes in either beryllium foil or actual target capsules using femtosecond laser pulses. We have the means to drill in a vacuum and have created holes using a flat-top beam. We have not yet attempted to drill small high-aspect ratio holes. Initial projections are that drilling a 1- μm -diameter hole 100 μm deep, without any taper, would be virtually impossible, but that drilling a 3- to 5- μm -diameter hole approximately 50 μm deep with very little taper, could probably be done with a minimum number of problems. Once the holes have been drilled, they can be photographed and compared to the holes already drilled using nanosecond pulse lengths.


Conclusions

From the information available, it does seem feasible to create micro-holes suitable for filling. Based on preliminary investigations, however, it does not seem likely that a commercial company will be able to produce these holes. SEM photos of commercially-drilled holes show an excessive amount of thermal damage due to laser pulse

lengths of relatively long durations (nanoseconds or longer). Furthermore, most commercial companies are not equipped with the appropriate lenses and laser set-up to drill <5- μm -sized holes, because the current demand is not high enough.

Initial studies indicate that using a laser capable of femtosecond pulses may help to eliminate the thermal damage caused by longer pulse length lasers and could prove beneficial in creating holes in ICF target capsules suitable for filling. Efforts are being made to have preliminary sample holes made at LLNL. Although not delineated in this report, studies are currently on-going to address the issues of sealing the holes, once drilled, and then polishing the capsules to produce the necessary surface finish required.

References

1. Korner, C., R. Mayerhofer, M. Hartmann, and H. W. Bergmann (1996), "Physical and material aspects in using visible laser pulses of nanosecond duration for ablation," *Applied Physics A*, **63**, pp. 123-131.
2. Luft, A., A. Franz, J. Emsermann, and J. Kaspar (1996), "A study of thermal and mechanical effects on materials induced by pulsed laser drilling," *Applied Physics A*, **63**, pp. 93-101.
3. Stuart, B. C., M. D. Feit, A. M. Rubenchik, B. W. Shore, and M. D. Perry (1995), "Physical Review Letters," March, Vol. **74** (12), pp. 2248-2251.
4. Chichkov, B. N., C. Momma, S. Nolte, F. von Alvensleben, and A. Tünnermann (1996), "Femtosecond, picosecond, and nanosecond laser ablation of solids," *Applied Physics A*, **63**, pp. 109-115.
5. Ihlemann, J., A. Scholl, H. Schmidt, and B. Wolff-Ronke (1995), "Nanosecond and femtosecond excimer-laser ablation of oxide ceramics," *Applied Physics A*, **60**, pp. 411-417.
6. Preuss, S., A. Demchuk, and M. Stuke (1995), "Sub-picosecond UV laser ablation of metals," *Applied Physics A*, **61**, pp. 33-37.
7. Momma, C., B. N. Chichkov, S. Nolte, F. von Alvensleben, A. Tünnermann, H. Welling, and B. Welleghausen (1996), "Short-pulse laser ablation of solid targets," *Optics Communications*, August, Vol. **128**, pp. 101-109.
8. Stuart, B. C., M. D. Perry, A. M. Rubenchik, J. Neev, S. Herman, H. Nguyen, P. Armstrong, and L. B. DaSilva (1997), "Femtosecond Laser Materials Processing," *CLEO, Glen Arm, MD*. 

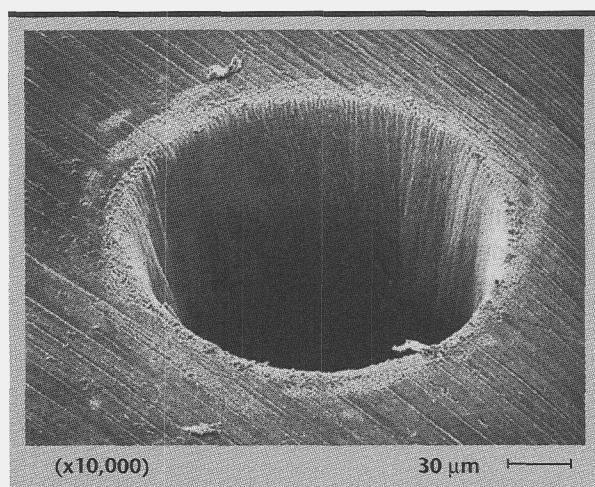


Figure 6. SEM photograph of hole drilled in 100- μm -thick steel, using a femtosecond laser.



Technical Information Department
Lawrence Livermore National Laboratory
University of California
Livermore, California 94551

